https://doi.org/10.48047/AFJBS.6.Si2.2024.6181-6192

African Journal of Biological Sciences

Journal homepage: http://www.afjbs.com

Research Paper Open Access

Investigation of Antimicrobial and Anticancer Activity of Fe_3O_4 Nanoparticles Coated With [BMIM] [BF_4] Ionic Liquid

Rajarajeswari A[1], Stella S[2*]

[1]Department of Chemistry & Research Centre, Sarah Tucker College (Autonomous) Affiliated to Manonmaniam Sundaranar University,Tirunelveli- 627 012,Tamil Nadu India.
[2*]Research Scholar (Reg. No. 18221202032006) Department of Chemistry, Tirunelveli Dakshina Mara Nadar Sangam College, T.Kallikulam, Affiliated to Manonmaniam Sundaranar University, Tirunelveli-627113, Tamil Nadu, India.

Email: [2*]stella@sarahtuckercollege.edu.in

Article Info

Volume 6, Issue Si2, May 2024

Received: 08 May 2024

Accepted: 15 June 2024

Published: 06 July 2024

doi:

10.48047/AFJBS.6.Si2.2024.6181-6192

ABSTRACT:

The current investigation involved the preparation of Iron (II, III) oxide nanoparticles (Fe_3O_4 NPs) and iron (II, III) oxide nanoparticles coated with 1-butyl-3-methylimidazolium tetrafluoroborate ([BMIM][BF_4]) ionic liquid (Fe_3O_4-[BMIM][BF_4] NPs) using co-precipitation method. These nanoparticles were analysed using X-ray diffraction (XRD), Fourier-transform infrared spectroscopy (FTIR), ultraviolet (UV) spectroscopy, and transmission electron microscopy (TEM). The Fe_3O_4-[BMIM][BF_4] NPs that were obtained exhibited a hexagonal crystal structure. Average crystallite size was calculated from XRD analysis such as Fe_3O_4 NPs was 15.3 nm, while the Fe_3O_4-[BMIM] [BF_4] NPs had an average size of 5.67 nm. The present study examined the application potential of produced nanoparticles for their antibacterial and anti-cancer activities using both the agar well diffusion method and the MTT assay, respectively. Out of the various types of microbial pathogens tested, the material showed the strongest ability to inhibit the growth of *Aspergillus favus* (9mm) and *Candida Albicans* (9mm) at a concentration 80 µg/ml. Additionally, the sample was also examined for its potential to combat breast cancer cells (MCF7) using the MTT assay. The observed cytotoxic effect exhibited a direct correlation with the concentration of the substance. The synthesized Fe_3O_4-[BMIM] [BF_4] nanoparticles have the potential for use in environmental and biomedical applications.

Keywords: Magnetite, Particle Size, MTT Assay, Ferric Chloride, Ferrous Chloride.

1. Introduction

Nanomaterials are commonly synthesised due to their distinct features, such as mechanical, optical, and magnetic properties, which differ from those of bulk materials [1–3]. Metal oxides are utilised in diverse applications such as catalysis, magnetic storage, and biological applications including bone tissue engineering [4–7]. The increasing life expectancy and ageing population have led to a growing demand for artificial materials to mend damaged bones [8–11]. Nanotechnology has addressed the dilemma by developing a range of ceramics that possess bioactivity [12], mechanical characteristics [13], and the capacity to stimulate bone development. Iron oxide powder at the nanoscale scale is extensively used due to advancements in preparation technology. The usage of monodispersed magnetite nanoparticles has greatly enhanced the application of magnetic nanoparticles in several fields such as Ferro fluids, biological imaging, and treatments [14, 15]. The compound Fe_3O_4, known as magnetic iron oxide, exhibits a face-centered cubic structure with a cubic inverse spinal arrangement. Within this structure, the iron (Fe) cations occupy both the interstitial tetrahedral sites and the octahedral sites [16]. At ambient temperature, the Fe^{2+} and Fe^{3+} ions undergo interconversion in the octahedral sites, resulting in the formation of a type of materials known as half-metallic minerals [17]. Magnetite nanoparticles can be synthesised using several chemical methods, such as co-precipitation of aqueous ferrous and ferric solutions [18], microemulsion technique [19], and hydrothermal synthesis [20], in order to achieve the appropriate physical and chemical properties. Superparamagnetic nanoparticles are extremely fascinating substances due to their use in magnetic resonance imaging (MRI) [21–23], medication administration [24], and cell isolation [25]. Metal nanoparticles are of great interest in the field of antibacterial drugs due to their ability to be synthesised with a large surface area and highly active sites. Iron oxide nanoparticles possess unique magnetic characteristics and exhibit exceptional biocompatibility, making them a distinct type of metal oxide.

Recently, extensive efforts have been made to develop novel medications in response to the growing resistance of microorganisms to existing treatments. This paper presents a unique method for synthesising Fe_3O_4 nanoparticles using a surfactant. Additionally, it aims to investigate the antibacterial properties of these nanoparticles.

2. Materials and methods

2.1 Materials

Ionic liquid, (1-butyl-3-methylimidazolium tetrafluoroborate) [BMIM] [BF_4] was purchased from Himedia with a purity above 99%. Ferric Chloride ($FeCl_3$), and Ferrous chloride ($FeCl_2$) Sodium hydroxide was obtained from Fine Laboratory Reagents. No further purification was performed on the compounds before using them at the analytical grade. The whole synthesis was carried using double-distilled water.

2.2. Synthesis of [BMIM] [BF_4] assisted ZnO NPs by Co-precipitation process

2.7 mmol of Ferric chloride ($FeCl_3$) together with 6.6 mmol of ferrous chloride ($FeCl_2$) were individually dissolved in 50 ml of water. Subsequently, the solutions were combined with 1 ml of [BMIM] [PF_6] ionic liquid. The metal salt was dissolved fully by aggressively stirring the solution using a magnetic stirrer. To continue the process at the basic pH around 11, 2M Sodium Hydroxide (NaOH) which was added dropwise to the reaction medium. After stirring for 1 h at a temperature of 70°C, a separate black suspension of Fe_3O_4 coated with IL were formed. Additionally, the reaction mixture was cooled to 35^0C and kept at a constant stirring

for 30 minutes. The Fe_3O_4-[BMIM][BF_4] precipitate was separated using centrifugation and any excess ions from the reactant component were thoroughly rinsed with distilled water many times to get [BMIM][BF_4] coated Fe_3O_4 NPs, the material that had been centrifuged was dried at a temperature of 80°C for a duration of 5 h. In the same way, bare metal oxide nanoparticles were synthesised using the procedure mentioned above, but without adding [BMIM] [BF_4].

3. Results and Discussion

Synthesized Fe_3O_4 NPs and Fe_3O_4-[BMIM][BF_4] NPs were evaluated in the following studies:

3.1. X-ray Diffraction Studies

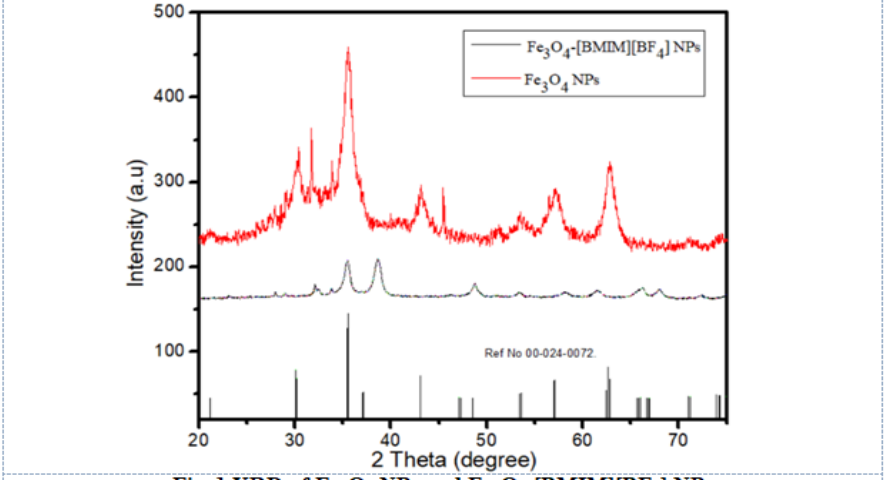

Fig. 1 XRD of Fe_3O_4 NPs and Fe_3O_4-[BMIM][BF_4] NPs

Fig. 1 shows the X-ray powder diffractograms of the Fe_3O_4 NPs and Fe_3O_4-[BMIM] [BF_4].

The XRD analysis was conducted to determine the crystallinity and phase of Fe_3O_4 NPs and Fe_3O_4-[BMIM][BF_4]. The diffraction peaks observed at Bragg angles of 32.26, 35.65, 37.25, 43.17, 47.12, 57.17 and 62.72 degrees correspond to the (104), (110), (006), (202), (122), and (214) planes respectively, for Fe_3O_4. The samples exhibit a hexagonal crystal structure and belong to either the C6v4 or P63mc space group (JCPDS 01-076-0704) [26]. a = b = 2.2530 Å, c = 5.2130 Å, $\alpha = \beta = 90^\circ$, and $\gamma = 120^\circ$ are the corresponding lattice parameter. The incorporation of IL into the Fe_3O_4 structure leads to substantial modifications in the peak position and intensity of Fe_3O_4-[BMIM][BF_4] NPs compared to Fe_3O_4-NPs. Significant peak broadening is observed when the BMIM.BF_4 IL is introduced into the Fe_3O_4 crystal structure. The observed alteration in the properties of X-ray diffraction peaks may be attributed to the interactions between the BMIM.BF_4 ionic liquid and Fe_3O_4-NPs. The decrease in intensity of Fe_3O_4 NPs peaks, due to the small particle size of the nanoparticle which was below the limit of detection of XRD. Moreover, the presence of the ionic liquid on the nanoparticle surface covered the diffraction peaks of the Fe_3O_4 NPs and decreased the peaks intensity. This aligns with the average crystallite size of the produced samples, which was estimated using Scherrer's equation. The size was found to be 15.3 nm for Fe_3O_4-NPs and 5.67 nm for Fe_3O_4-[BMIM][BF_4] NPs . The crystallite size, have been computed by considering the conspicuous peaks at 33°, 35°, 43°, 53°, and 62°. The incorporation of BMIM.BF_4 IL into Fe_3O_4 NPs leads to a decrease in crystallite size. The decrease in crystallite size which is the function of IL which act as a surfactant that restricts the growth of Fe_3O_4 NPs.

The crystallite size was determined using the Scherer equation [27], which is expressed as follows:

$$D = K\lambda / \beta \cos\theta$$

The symbol D is size of the crystallite, λ is the wavelength of X-ray, K represents the crystallite form factor (0.94), and β represents the line broadening at half of the highest intensity.

3.2 FT-IR Spectra

Fig.2 reveal the FT-IR spectroscopy used to determine the structure and measurement of the chemical species in 450–4000 cm−1 wave number. Fe_3O_4 superparamagnetic nanoparticles exhibit absorption bands at 420-446 and 581-629 cm−1. The basic vibration modes are shown in Fig.2. The N-H stretching band and O-H from ethanol and water may be responsible for the absorption about 3413 cm−1. The Fe-O band has a low energy interval between 1382 cm−1 and 1000 cm−1, whereas water's O-H band bends at 1609 cm−1. The absorption bands from 2861 to 2965 cm−1 correspond to symmetric stretching vibration and asymmetrical C-H group (Imidazolium ring), respectively, whereas the band at 1480 cm−1 is connected with methylene [28].

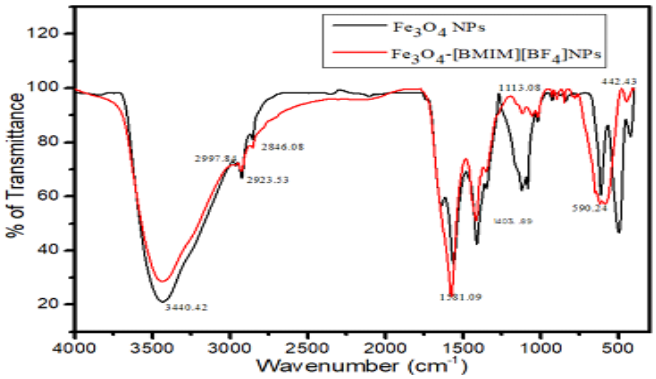

Fig. 2 FT-IR of Fe_3O_4 NPs and Fe_3O_4-[BMIM][BF_4] NPs

Furthermore, the band at 3418 cm^{-1} represents the secondary amino group's bending vibration [29]. The ionic liquid coating lowered the strength of the bending vibration band and almost eliminated the stretching band in Fe_3O_4 NPs, The\ absorbed peaks were at 1623.90 cm^{-1} and 1401.46 cm^{-1}, respectively. These values match the vibration modes of Fe_3O_4 and pure magnetite [30]. The FTIR spectra revealed no peaks that would have indicated contamination in the material.

3.3 UV-Vis Spectral Studies

UV-Vis spectroscopy is very valuable for analysing localised surface plasmon resonance (SPR). This instrument allows for the determination of absorption strength at various wavelengths of light. The wavelengths of ultraviolet and visible light may disrupt the surface electrons of the magnetite nanoparticles. The absorption peak provides information on the dimensions, magnitude, and distribution of the nanoparticles in terms of their scale, size, and shape [31]. Fig. 3a & 3c displays the surface plasmon resonance (SPR) for magnetite nanoparticles that have been synthesised. The study was focused on spherical monodisperse particles, and it was observed that the peak wavelength shifted to a shorter value (from 374 nm to 370 nm) upon adding the solution of ionic liquid [32]. Fig. 3 illustrates the relationship between the location of the absorbance peak and the intensity of surface plasmon resonance (SPR) for Fe_3O_4 NPs and Fe_3O_4-[BMIM] [BF_4] NPs. The aim is to get a shorter wavelength,

which corresponds to smaller particle size [33], while maintaining optimal absorbance intensity.

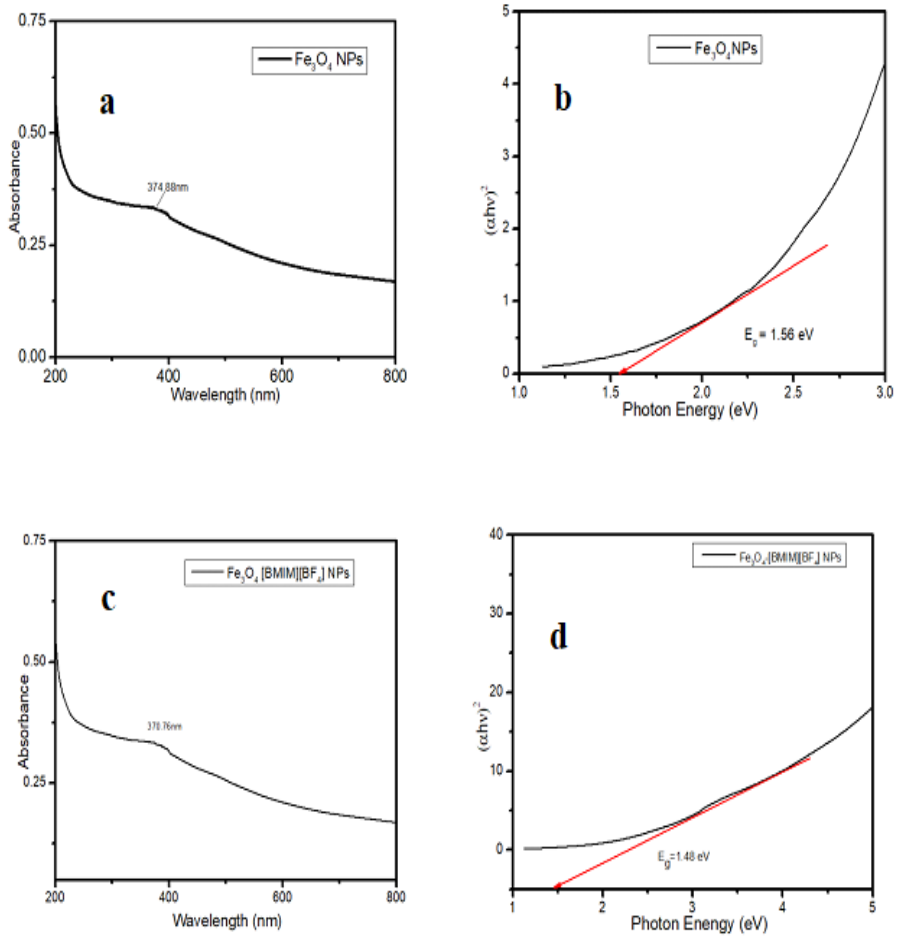

Fig.3 Absorption spectra of a) Fe $_3O_4$ NPs, b) Fe $_3O_4$-[BMIM][BF_4] NPs c) Bandgap energy of Fe_3O_4 NPs, d) Bandgap energy of Fe_3O_4-[BMIM][BF_4] NPs

Optical band gap of synthesised nanoparticles with and without the addition of IL are revealed in fig. 3a & 3b. The band gaps energy of Fe_3O_4 NPs and Fe_3O_4-[BMIM] [BF_4] NPs are 1.56 eV and 1.48 eV respectively. Evidence demonstrates that the interaction between [BMIM][BF_4] and Fe_3O_4 NPs leads to a decrease of the band gap. Quantum confinement is the prime reason for decrease of particle size and lowering of band gap due to the incorporation of IL to Fe_3O_4 NPs. Results showed that with a reduction in particle size from a bulk value, the band gap dropped to a specific minimum value. It is conceivable that the band gap changes in relation to particle size because of the delocalization of molecular orbitals at the conduction band edge caused by the bulk defects. This leads to the formation of shallow and deep electronic energy traps, which in turn causes the absorption spectra to redshift. The absorption spectra blue-shifted as a consequence of the traps changing to higher energy when the crystallite size shrank below its size at the band gap minimum.

3.4 TEM

The transmission electron microscopy (TEM) pictures of the synthesised Fe_3O_4-[BMIM][BF_4] NPs can be shown in Figure 4a –c. TEM was used to analyse the particle size and surface morphology of IL-coated Fe_3O_4 NPs. The findings indicated that the Fe_3O_4-

[BMIM][BF_4] NPs exhibited a polydisperse distribution and had a spherical shape. The SAED pattern verified the crystal structure of Fe_3O_4-[BMIM][BF_4] NPs. The SAED patterns indicate that Fe_3O_4-[BMIM] [BF_4] NPs exhibit unique lattice fringes that resemble those of regular IL-coated Fe_3O_4 NPs and they possess exceptional crystalline quality.

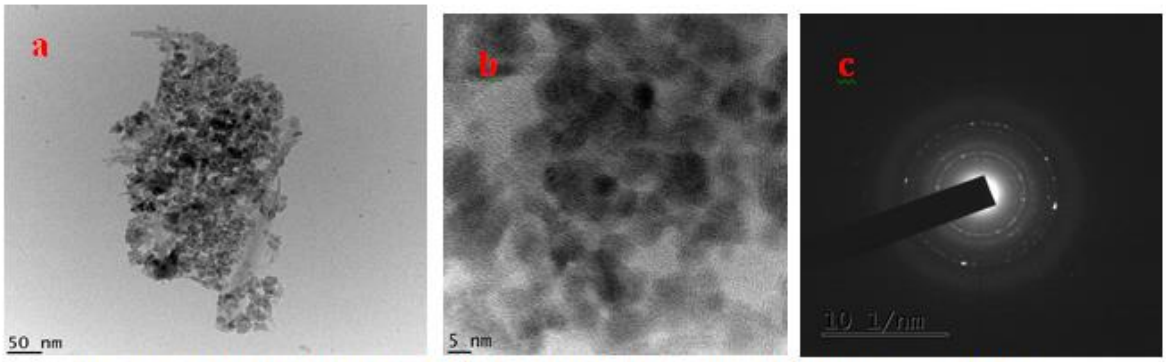

Fig. 4 a) & b) HR-TEM Fe_3O_4-[BMIM][BF_4] NPs c) SAED Pattern of Fe_3O_4-[BMIM][BF_4] NPs

3.5 Anti- Microbial Activity

The antibacterial activity of Fe_3O_4-[BMIM][BF_4] NPs against bacterial and fungal pathogens, including Staphylococcus aureus, Pseudomonas aeruginosa, Aspergillus favus, and Candida albicans, was investigated using the disc diffusion technique (Fig. 5a -d).

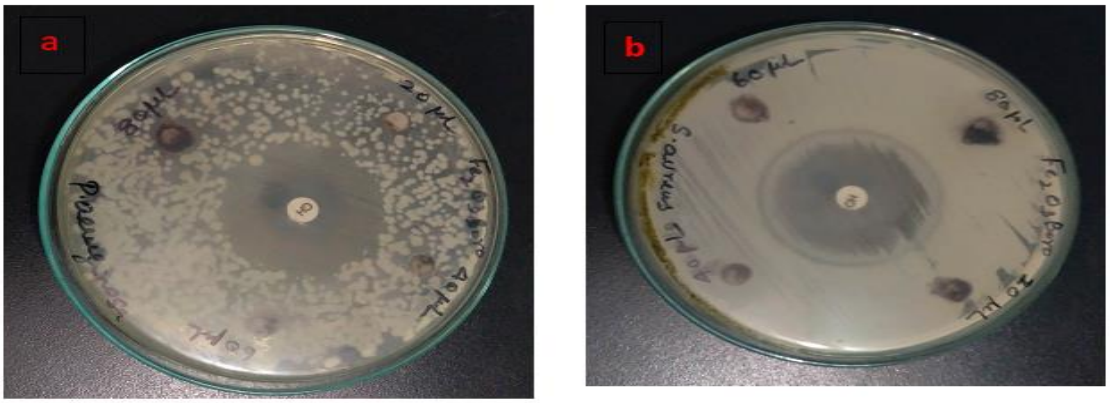

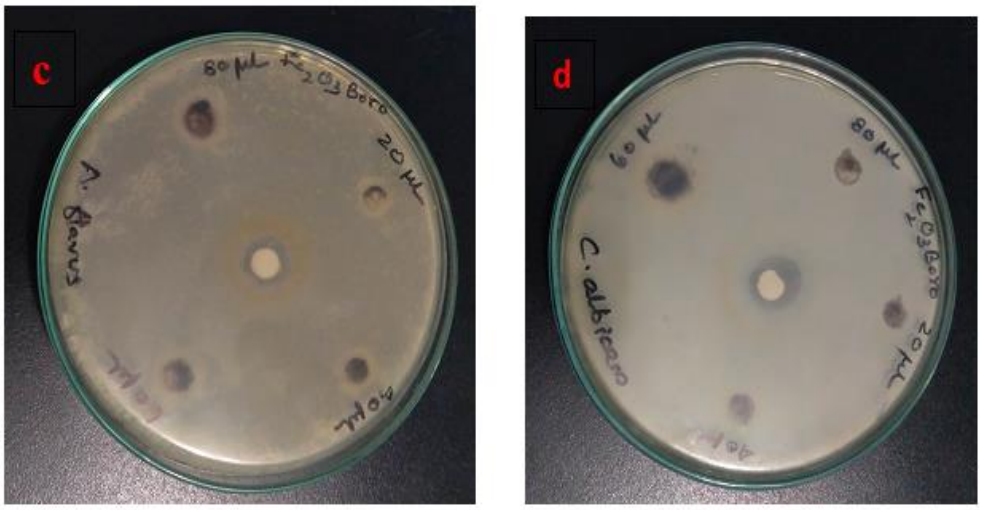

Fig. 5 Inhibition zone showing the antibacterial activity against a) *Staphylococcus aureus, b) Pseudomonas aeruginosa, c) Aspergillus favus,* d) Candida *albicans* respectively, of Fe_3O_4-[BMIM][BF_4] NPs

In lab, nutritious broth is often used to support the growth of live bacterial pathogens (as subcultures with a turbidity of 0.5 Mc) that have been cultured overnight at 37 °C. The newly cultivated bacterial culture was equally spread on sterilised Petri plates with nutrient agar. Fe_3O_4-[BMIM] [BF_4] NPs (20, 40, 60, and 80 µL) were deposited onto the clean discs. Amikacin discs were used as a control. All plates were incubated at 37 °C for 24-48 hours to observe the formation of a bacterial inhibition zone around the disc.

The reported zone of inhibition for the bacterium Staphylococcus aureus was 12.0 mm, for Pseudomonas aeruginosa it was 13.0 mm, for Aspergillus favus it was 9.0 mm, and for Candida Albicans it was also 9.0 mm. The Fe_3O_4-[BMIM] [PF_6] had lower efficacy against the bacteria compared to fungi.

The mechanism by which Fe_3O_4-[BMIM] [BF_4] NPs exhibits antibacterial action is the dependence of NPs is contingent upon the dimensions, arrangement, and amount of copper oxide [34]. There are three primary modes in which antibacterial action occurs. (1) Cell wall and membrane degeneration, (2) Infiltration and disruption of cells, and (3) Oxidative stress [35]. The Fe_3O_4-[BMIM] [BF_4] NPs exhibited antibacterial action against each microorganism.is shown in Table 1.

Table 1. Antimicrobial action of Fe_3O_4-[BMIM][BF_4] NPs

S.NO	**Bacterial Pathogen**	**Anti- Bacterial activity—zone of growth inhibition (mm)**				
		20µL	40µL	60µL	80µL	Control
1.	*Staphylococcus aureus*	7	9	10	12	25
2.	*Pseudomonas aeruginosa*	9	9	11	13	30
S.NO	Fungal Pathogen	Anti- Fungal activity—zone of growth inhibition (mm)				
		20µL	40µL	60µL	80µL	Control
1.	Aspergillus favus	7	7	7	9	13
2.	Candida Albicans	7	9	9	9	12

3.6 Anti-Cancer Activity

The harmful effects of Fe_3O_4 [BMIM] [BF_4] NPs on human MCF7 Breast cancer cells were assessed at different doses ranging from 0 to 500 µg/mL. The cell proliferation was assessed using an inverted phase contrast microscope. Microscopic images of MCF7 cells post-treatment with Fe_3O_4 [BMIM] [BF_4] NPs are shown fig. 6. Nucleoplasmic proteins (NPs) exhibited cellular contraction, as well as the presence of condensed and fragmented nuclie in the presence of nanoparticles [36].

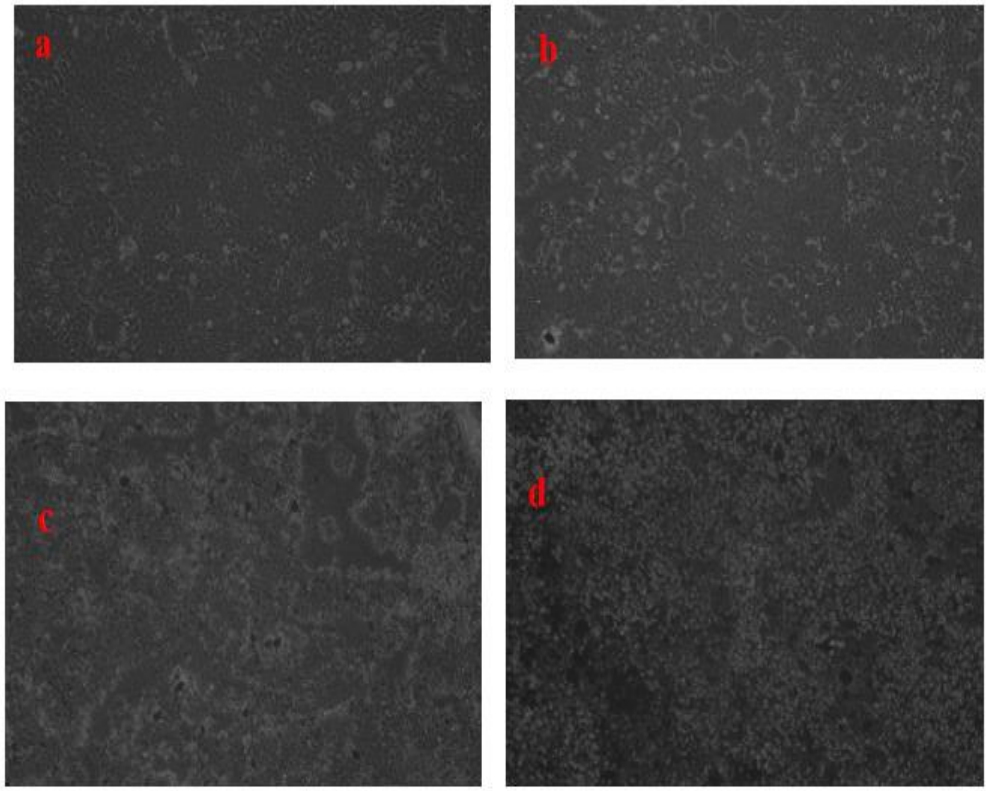

Fig. 7 Evaluation of cell survival and morphology. Evaluation of cell survival and morphology. Survival (%) of MCF7 human breast cancer cells upon exposure to different concentrations a. control b. 125 µg/mL c. 250 µg/mL d. 500 µg/mL

Noticeable alterations in morphology were seen at different doses of Fe_3O_4-[BMIM][BF_4]NPs. The substance exhibited cytotoxic effects on MCF7 cancer cells in a way that was dependent on its concentration [37], as shown by the data presented in Fig. 7. A concentration of 97.14 µg/mL of Fe_3O_4-[BMIM] [BF_4] NPs nanoparticles resulted in 50% cell killing, which is known as the IC50 value.

The size and dose of nanoparticles are crucial factors in causing toxicity [38]. Fig. 8 depicts the percentage inhibition of Fe_3O_4 [BMIM] [BF_4] NPs against human breast cancer MCF-7 cell lines. Nanoparticles enter cells by many mechanisms, including clathrin-mediated transport, caveolae-dependent endocytosis, and macro-pinocytotic uptake endocytosis [39]. Upon entering the cell, magnetite nanoparticles have the ability to directly engage with NADPH oxidases found in the plasma membrane and/or mitochondria, leading to the production of superoxide ion [40, 41]. As a result, this process triggers redox-sensitive signalling which then cause pro-inflammatory effects and cytotoxicity [42, 43].

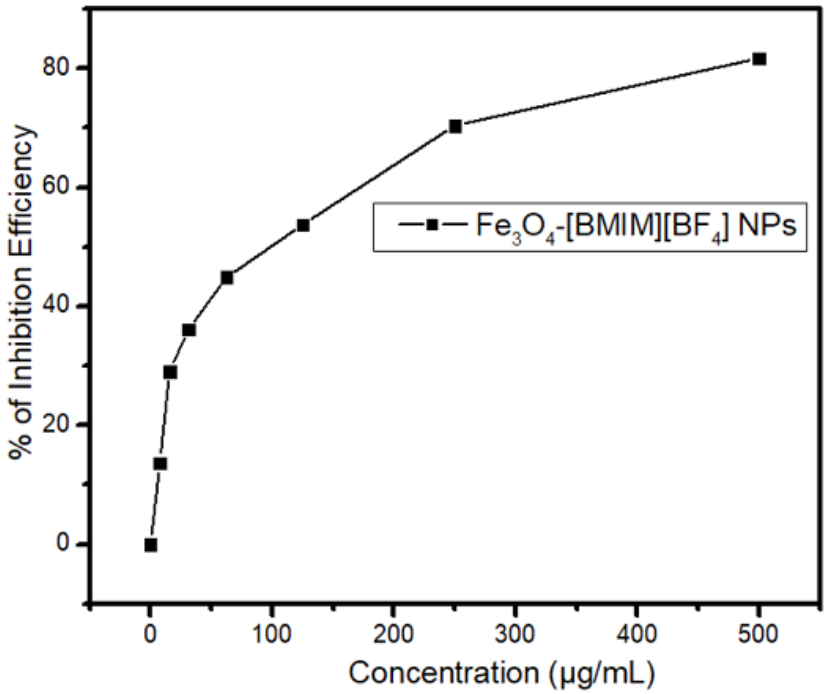

Fig 8. Cytotoxicity of Fe_3O_4- [BMIM][BF_4] nanoparticles on human breast cancer MCF-7 cell lines

4. Conclusion

This current study aims to synthesize Fe_3O_4 nanoparticles with distinct optical and structural properties. These nanoparticles were effectively synthesized along with the ionic liquid [BMIM] [BF_4] utilizing the co-precipitation approach. This work involved a comparison of Fe_3O_4 nanoparticles (NPs) that were created with and without an ionic liquid (IL) coating. The objective was to assess the influence of imidazolium-based ILs on the structure and optical properties of Fe_3O_4 NPs. The XRD study indicated crystallite sizes of 15.3 nm for Fe_3O_4-NPs and 5.67 nm for Fe_3O_4-[BMIM] [BF_4] NPs, confirming the formation of a hexagonal crystal structure. The FTIR spectra offer compelling evidence for the synthesized Fe_3O_4-NPs and Fe_3O_4-[BMIM] [BF_4] NPs. The quantum confinement effect demonstrated by NPs led to a decrease in the band gap energy. Consequently, the [BMIM][BF_4] IL stimulates the synthesis of modified Fe_3O_4-NPs. The size and form of the synthesized sample were evaluated using HR-TEM analysis. The proliferation of *Candida albicans*, a fungal microorganism, was shown to be suppressed by Fe_3O_4-[BMIM][BF_4] IL NPs, but the growth of *Pseudomonas aeruginosa* and *Staphylococcus aureus*, two bacterial pathogens, was only slightly affected. The synthesized sample demonstrated a significant inhibitory activity of 97.17% against the cancer cell line.

5. Reference

1. Baig, N., Kammakakam, I., & Falath, W. (2021). Nanomaterials: A review of synthesis methods, properties, recent progress, and challenges. Materials Advances, 2(6), 1821-1871.

2. Joudeh, N., & Linke, D. (2022). Nanoparticle classification, physicochemical properties, characterization, and applications: a comprehensive review for biologists. Journal of Nanobiotechnology, 20(1), 262.
3. Salem, S. S., Hammad, E. N., Mohamed, A. A., & El-Dougdoug, W. (2022). A comprehensive review of nanomaterials: Types, synthesis, characterization, and applications. Biointerface Res. Appl. Chem, 13(1), 41.
4. Eivazzadeh-Keihan, R., Bahojb Noruzi, E., Khanmohammadi Chenab, K., Jafari, A., Radinekiyan, F., Hashemi, S. M., ... & Hamblin, M. R. (2020). Metal-based nanoparticles for bone tissue engineering. Journal of Tissue Engineering and Regenerative Medicine, 14(12), 1687-1714.
5. Singh, K. R., Nayak, V., Singh, J., Singh, A. K., & Singh, R. P. (2021). Potentialities of bioinspired metal and metal oxide nanoparticles in biomedical sciences. RSC advances, 11(40), 24722-24746.
6. Nikolova, M. P., & Chavali, M. S. (2020). Metal oxide nanoparticles as biomedical materials. Biomimetics, 5(2), 27.
7. Mujahid, M. H., Upadhyay, T. K., Khan, F., Pandey, P., Park, M. N., Sharangi, A. B., ... & Kim, B. (2022). Metallic and metal oxide-derived nanohybrid as a tool for biomedical applications. Biomedicine & Pharmacotherapy, 155, 113791.
8. Gorejová, R., Haverová, L., Oriňaková, R., Oriňak, A., & Oriňak, M. (2019). Recent advancements in Fe-based biodegradable materials for bone repair. Journal of Materials Science, 54(3), 1913-1947.
9. Arcos, D., Boccaccini, A. R., Bohner, M., Díez-Pérez, A., Epple, M., Gómez-Barrena, E., ... & Vallet-Regí, M. (2014). The relevance of biomaterials to the prevention and treatment of osteoporosis. Acta biomaterialia, 10(5), 1793-1805.
10. Babuska, V., Kasi, P. B., Chocholata, P., Wiesnerova, L., Dvorakova, J., Vrzakova, R., ... & Kulda, V. (2022). Nanomaterials in bone regeneration. Applied Sciences, 12(13), 6793.
11. Gautam, S., Bhatnagar, D., Bansal, D., Batra, H., & Goyal, N. (2022). Recent advancements in nanomaterials for biomedical implants. Biomedical Engineering Advances, 3, 100029.
12. Butler, J., Handy, R. D., Upton, M., & Besinis, A. (2023). Review of antimicrobial nanocoatings in medicine and dentistry: mechanisms of action, biocompatibility performance, safety, and benefits compared to antibiotics. ACS nano, 17(8), 7064-7092.
13. Ariga, K., Minami, K., Ebara, M., & Nakanishi, J. (2016). What are the emerging concepts and challenges in NANO? Nanoarchitectonics, hand-operating nanotechnology and mechanobiology. Polymer journal, 48(4), 371-389.
14. Shabatina, T. I., Vernaya, O. I., Shabatin, V. P., & Melnikov, M. Y. (2020). Magnetic nanoparticles for biomedical purposes: Modern trends and prospects. Magnetochemistry, 6(3), 30.
15. Colombo, M., Carregal-Romero, S., Casula, M. F., Gutiérrez, L., Morales, M. P., Böhm, I. B., ... & Parak, W. J. (2012). Biological applications of magnetic nanoparticles. Chemical Society Reviews, 41(11), 4306-4334.
16. Shultz, M. D. (2008). Magnetic Nanoparticles Based on Iron: Synthesis, Characterization, Design, and Application.
17. Hamed, M. H. A. (2021). Interface functionalization of magnetic oxide Fe3O4/$SrTiO_3$ heterostructures. Forschungszentrum Jülich GmbH.
18. Ganapathe, L. S., Mohamed, M. A., Mohamad Yunus, R., & Berhanuddin, D. D. (2020). Magnetite (Fe_3O_4) nanoparticles in biomedical application: From synthesis to surface functionalisation. Magnetochemistry, 6(4), 68.

19. Unsoy, G., Gunduz, U., Oprea, O., Ficai, D., Sonmez, M., Radulescu, M., ... & Ficai, A. (2015). Magnetite: from synthesis to applications. Current topics in medicinal chemistry, 15(16), 1622-1640.
20. Yusefi, M., Shameli, K., & Jumaat, A. F. (2020). Preparation and properties of magnetic iron oxide nanoparticles for biomedical applications: A brief review. Journal of Advanced Research in Materials Science, 75(1), 10-18.
21. Dulińska-Litewka, J., Łazarczyk, A., Hałubiec, P., Szafrański, O., Karnas, K., & Karewicz, A. (2019). Superparamagnetic iron oxide nanoparticles—Current and prospective medical applications. Materials, 12(4), 617.
22. Wahajuddin, N., & Arora, S. (2012). Superparamagnetic iron oxide nanoparticles: magnetic nanoplatforms as drug carriers. International journal of nanomedicine, 3445-3471.
23. Mahmoudi, M., Hosseinkhani, H., Hosseinkhani, M., Boutry, S., Simchi, A., Journeay, W. S., ... & Laurent, S. (2011). Magnetic resonance imaging tracking of stem cells in vivo using iron oxide nanoparticles as a tool for the advancement of clinical regenerative medicine. Chemical reviews, 111(2), 253-280.
24. Pucci, C., Degl'Innocenti, A., Gümüş, M. B., & Ciofani, G. (2022). Superparamagnetic iron oxide nanoparticles for magnetic hyperthermia: recent advancements, molecular effects, and future directions in the omics era. Biomaterials Science, 10(9), 2103-2121.
25. Sezer, N., Arı, İ., Bicer, Y., & Koc, M. (2021). Superparamagnetic nanoarchitectures: Multimodal functionalities and applications. Journal of Magnetism and Magnetic Materials, 538, 168300.
26. Zarrabi, M., Haghighi, M., Alizadeh, R., & Mahboob, S. (2022). Hybrid sonoprecipitation fabrication of magnetic ZnO-GO-Fe_3O_4 nanophotocatalyst for solar-light-driven degradation of dyes in water. Materials Research Bulletin, 153, 111907.
27. Mustapha, S., Ndamitso, M. M., Abdulkareem, A. S., Tijani, J. O., Shuaib, D. T., Mohammed, A. K., & Sumaila, A. (2019). Comparative study of crystallite size using Williamson-Hall and Debye-Scherrer plots for ZnO nanoparticles. Advances in Natural Sciences: Nanoscience and Nanotechnology, 10(4), 045013.
28. Sundrarajan, M., & Ramalakshmi, M. (2012). Novel cubic magnetite nanoparticle synthesis using room temperature ionic liquid. Journal of Chemistry, 9, 1070-1076.
29. Chandra, S., Saleem, H., Erdogdu, Y., Subashchandrabose, S., Krishnan, A. R., & Gulluoglu, M. T. (2011). FT-IR, FT-Raman spectra and scaled quantum mechanical study of 4-amino-1-benzylpiperidine. Journal of molecular structure, 998(1-3), 69-78.
30. Bahari, A. (2017). Characteristics of Fe 3 O 4, α-Fe 2 O 3, and γ-Fe 2 O 3 nanoparticles as suitable candidates in the field of nanomedicine. Journal of Superconductivity and Novel Magnetism, 30, 2165-2174.
31. Grand, J., Auguié, B., & Le Ru, E. C. (2019). Combined extinction and absorption UV–visible spectroscopy as a method for revealing shape imperfections of metallic nanoparticles. Analytical chemistry, 91(22), 14639-14648.
32. Das, A. K., Solanki, V. S., Fanan, A., Agarwal, N., & Yadav, V. K. (2024). Plant protein-mediated size-controlled synthesis of magnetite nanoparticles–Studies on optical properties. Bulletin of the Chemical Society of Ethiopia, 38(2), 493-499.
33. Casula, M. F., Jun, Y. W., Zaziski, D. J., Chan, E. M., Corrias, A., & Alivisatos, A. P. (2006). The concept of delayed nucleation in nanocrystal growth demonstrated for the case of iron oxide nanodisks. Journal of the American Chemical Society, 128(5), 1675-1682..
34. Majumdar, T. D., Singh, M., Thapa, M., Dutta, M., Mukherjee, A., & Ghosh, C. K. (2019). Size-dependent antibacterial activity of copper nanoparticles against

Xanthomonas oryzae pv. oryzae–A synthetic and mechanistic approach. Colloid and Interface Science Communications, 32, 100190.

35. Godoy-Gallardo, M., Eckhard, U., Delgado, L. M., de Roo Puente, Y. J., Hoyos-Nogués, M., Gil, F. J., & Perez, R. A. (2021). Antibacterial approaches in tissue engineering using metal ions and nanoparticles: From mechanisms to applications. Bioactive Materials, 6(12), 4470-4490.
36. Sohrabi Kashani, A., & Packirisamy, M. (2021). Cancer-nano-interaction: From cellular uptake to mechanobiological responses. International Journal of Molecular Sciences, 22(17), 9587.
37. Lungu, I. I., Nistorescu, S., Badea, M. A., Petre, A. M., Udrea, A. M., Banici, A. M., ... & Balaş, M. (2020). Doxorubicin-conjugated iron oxide nanoparticles synthesized by laser pyrolysis: in vitro study on human breast cancer cells. Polymers, 12(12), 2799.
38. Naz, S., Gul, A., & Zia, M. (2020). Toxicity of copper oxide nanoparticles: a review study. IET nanobiotechnology, 14(1), 1-13.
39. Detampel, P., Tehranian, S., Mukherjee, P., Foret, M., Fuerstenhaupt, T., Darbandi, A., ... & Amrein, M. (2022). Caveolin-initiated macropinocytosis is required for efficient silica nanoparticles' transcytosis across the alveolar epithelial barrier. Scientific Reports, 12(1), 9474.
40. Pucci, C., Degl'Innocenti, A., Gümüş, M. B., & Ciofani, G. (2022). Superparamagnetic iron oxide nanoparticles for magnetic hyperthermia: recent advancements, molecular effects, and future directions in the omics era. Biomaterials Science, 10(9), 2103-2121.
41. Canaparo, R., Foglietta, F., Limongi, T., & Serpe, L. (2020). Biomedical applications of reactive oxygen species generation by metal nanoparticles. Materials, 14(1), 53.
42. Min, Y., Suminda, G. G. D., Heo, Y., Kim, M., Ghosh, M., & Son, Y. O. (2023). Metal-based nanoparticles and their relevant consequences on cytotoxicity cascade and induced oxidative stress. Antioxidants, 12(3), 703.
43. Makhdoumi, P., Karimi, H., & Khazaei, M. (2020). Review on metal-based nanoparticles: role of reactive oxygen species in renal toxicity. Chemical Research in Toxicology, 33(10), 2503-2514.